

PCCP

Accepted Manuscript



This is an *Accepted Manuscript*, which has been through the Royal Society of Chemistry peer review process and has been accepted for publication.

Accepted Manuscripts are published online shortly after acceptance, before technical editing, formatting and proof reading. Using this free service, authors can make their results available to the community, in citable form, before we publish the edited article. We will replace this *Accepted Manuscript* with the edited and formatted *Advance Article* as soon as it is available.

You can find more information about *Accepted Manuscripts* in the [Information for Authors](#).

Please note that technical editing may introduce minor changes to the text and/or graphics, which may alter content. The journal's standard [Terms & Conditions](#) and the [Ethical guidelines](#) still apply. In no event shall the Royal Society of Chemistry be held responsible for any errors or omissions in this *Accepted Manuscript* or any consequences arising from the use of any information it contains.

Role of the Reaction of Stabilized Criegee Intermediates with Peroxy
Radicals in Particle Formation and Growth in Air

Yue Zhao, Lisa M. Wingen, Véronique Perraud, John Greaves, and Barbara J.
Finlayson-Pitts*

Department of Chemistry, University of California, Irvine, CA, 92697

Revision for:

Physical Chemistry Chemical Physics

April 13, 2015

*Corresponding author: Email: bjfinlay@uci.edu; phone: (949) 824-7670; fax: (949)
824-2420

1 Abstract

2 Ozonolysis of alkenes is an important source of secondary organic aerosol (SOA) in
3 the atmosphere. However, the mechanisms by which stabilized Criegee
4 intermediates (SCI) react to form and grow the particles, and in particular the
5 contributions from oligomers, are not well understood. In this study, ozonolysis of
6 *trans*-3-hexene (C₆H₁₂), as a proxy for small alkenes, was investigated with an
7 emphasis on the mechanisms of particle formation and growth. Ozonolysis
8 experiments were carried out both in static Teflon chambers (18-20 min reaction
9 times) and in a glass flow reactor (24 s reaction time) in the absence and presence of
10 OH or SCI scavengers, and under different relative humidity (RH) conditions. The
11 chemical composition of polydisperse and size-selected SOA particles was probed
12 using different mass spectrometric techniques and infrared spectroscopy.
13 Oligomers having SCI as the chain unit are found to be the dominant components of
14 such SOA particles. The formation mechanism for these oligomers suggested by
15 our results follows the sequential addition of SCI to organic peroxy (RO₂) radicals,
16 in agreement with previous studies. Smaller particles are shown to have a
17 relatively greater contribution from longer oligomers. Higher O/C ratios are
18 observed in smaller particles and are similar to those of oligomers resulting from
19 RO₂ + *n* SCI, supporting a significant role for longer oligomers in particle nucleation
20 and early growth. Under atmospherically relevant RH of 30-80%, water vapor
21 suppresses oligomer formation through scavenging SCI, but also enhances particle
22 nucleation. Under humid conditions, or in the presence of formic or hydrochloric
23 acid as SCI scavengers, peroxyhemiacetals are formed by the acid-catalyzed particle
24 phase reaction between oligomers from RO₂ + *n* SCI and a *trans*-3-hexene derived
25 carbonyl product. In contrast to the ozonolysis of *trans*-3-hexene, oligomerization
26 involving RO₂ + *n* SCI does not appear to be prevalent in the ozonolysis of
27 α -cedrene (C₁₅H₂₄), indicating different particle formation mechanisms for small and
28 large complex alkenes that need to be taken into account in atmospheric models.

29 Introduction

30 Organic aerosol makes up a substantial fraction (20-90%) of submicron particles in
31 the atmosphere,¹⁻³ of which up to 90% is secondary organic aerosol (SOA).^{2,4} SOA
32 is produced by atmospheric oxidation of volatile organic compounds (VOCs) that
33 can lead to the formation of products having sufficiently low vapor pressures to
34 either nucleate to form new particles or condense onto pre-existing particles.^{5,6} At
35 present, however, a quantitative understanding of SOA formation from such
36 oxidation processes remains limited, resulting in large uncertainties in predicting the
37 impacts of organic aerosol on air quality, climate and human health.^{1-3,7-9}

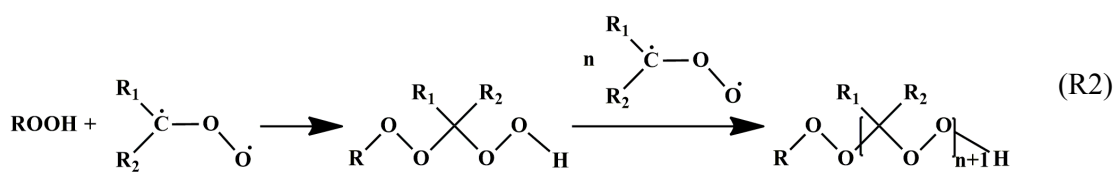
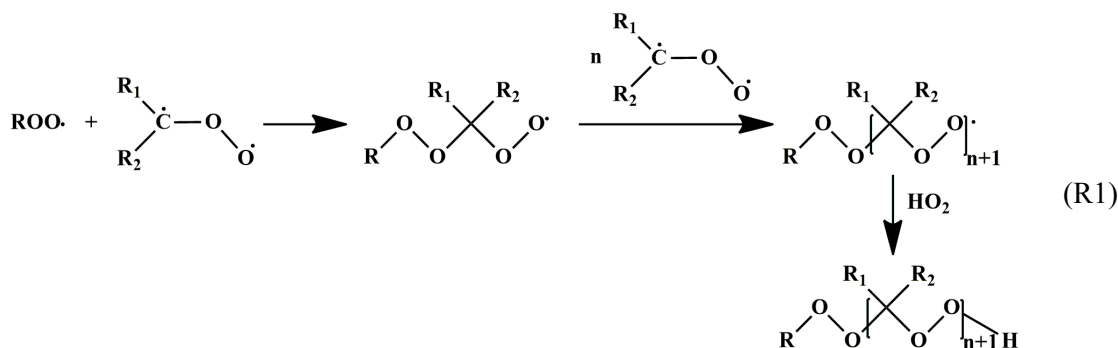
38 Ozonolysis of alkenes is an important source of SOA in the atmosphere.^{1,5,6,10,11}
39 Ozone-alkene reactions are known to proceed via the formation of a primary ozonide
40 which decomposes to a carbonyl product and a biradical/zwitterion known as the
41 Criegee intermediate.^{5,6,10} Over the past decades, special attention has been given
42 to the ozonolysis of large biogenic VOCs such as monoterpenes and
43 sesquiterpenes,^{1,3,10} which have structures and large molecular masses that favor the
44 formation of low volatility products upon atmospheric oxidation. Recently, high
45 molecular weight oligomers have been recognized as major constituents of SOA
46 from ozonolysis of large alkenes ($\geq C_{10}$).^{1,12-18} However, the identity of these
47 oligomers and their formation mechanisms are not well understood. Several
48 pathways leading to oligomer formation have been suggested, including (i) reactions
49 of stabilized Criegee intermediates (SCI) with carboxylic acids and carbonyls,
50 forming α -acyloxy hydroperoxides and secondary ozonides, respectively,^{12,15,18-20} (ii)
51 reactions of monomer products from ozonolysis, *e.g.*, aldol condensation,
52 peroxyhemiacetal formation, gem-diol formation, esterification, acetal and
53 hemiacetal formation;^{13,16,18,21-26} and (iii) formation of non-covalently bound dimer
54 clusters of carboxylic acids.^{21,26-28} Pathway (i) is thought to take place in the gas
55 phase, and pathway (ii) is suggested to occur mainly on the surface or within the
56 bulk of SOA particles, whereas pathway (iii) may occur in both phases. Quite
57 recently, gas phase formation of esters¹⁷ and highly oxidized products (termed as

58 extremely low-volatility organic compounds, ELVOCs)²⁹⁻³² have been suggested in
59 the α -pinene/O₃ system. The formation of ELVOCs possibly involves
60 intramolecular isomerization of RO₂ radicals.^{30,32-35}

61 There is growing evidence that oligomers play a key role in initial particle
62 formation from large alkenes because of their predicted very low vapor
63 pressures.^{19,36} In ozonolysis experiments where SCI were scavenged using small
64 acids or water, particle nucleation was shown to be suppressed, suggesting that the
65 oligomers formed from SCI were potentially the nucleating precursors.^{19,20,37} In an
66 α -pinene/O₃ system, the formation of 10-20 nm particles was well correlated with
67 gas phase oxidation products of high molecular weight (MW) (430-560 Da), whereas
68 particles larger than 20 nm were correlated with those having lower MW (140-380
69 Da).³¹ In a similar system, the gas phase formation of high MW ester dimers was
70 shown to be correlated with new particle formation in the presence of inorganic seed
71 particles.¹⁷ In another study, ELVOCs, which have been detected in both chamber
72 experiments and ambient air,²⁹⁻³² were suggested to be capable of acting as
73 nano-condensation nuclei and driving the formation of 3 nm particles.³⁰ It has also
74 been demonstrated, by measuring the composition of α -pinene/O₃ SOA particles
75 using mass spectrometry, that smaller particles contain more higher MW
76 components³⁸ and lower volatility carboxylic acids,³⁹ than do larger particles. This is
77 consistent with the role of oligomers in the initial stages of particle formation.

78 Formation of oligomers has also been reported for ozonolysis of small alkenes (<
79 C₆).⁴⁰⁻⁴⁴ For example, chamber studies of ozonolysis of isoprene have shown the
80 formation of oligomers in SOA through interspecies reactions of small oxidation
81 products such as aldehydes and carboxylic acids in the condensed phase, including
82 through aldol condensation, hemiacetal formation, and esterification.^{40,41} Accurate
83 mass measurements suggested that these oligomers have high oxygen content
84 (average O/C = 0.6) and comprise the majority of isoprene/O₃ derived SOA.⁴⁰
85 Recently, theoretical^{45,46} and experimental⁴¹⁻⁴⁴ studies have suggested the gas phase
86 formation of low-volatility oligomers containing SCI as the repeat unit during the

87 ozonolysis of small enol ethers and alkenes (including isoprene) in dry air. Two
 88 different mechanisms have been proposed: sequential addition of SCI to peroxy
 89 radicals (RO_2) (Reaction R1),⁴³ or to hydroperoxides (ROOH) (Reaction R2).⁴⁴



90 Sadezky *et al.*⁴³ investigated the formation of oligomers from the ozonolysis of a
 91 number of simple alkenes including *trans*-3-hexene in a static chamber, and
 92 proposed the structures and mechanisms shown in reaction (R1). We report here an
 93 expanded investigation of the ozonolysis of *trans*-3-hexene in which particle
 94 composition is probed as a function of size. In addition, the influence of water
 95 vapor, OH and SCI scavengers, as well as the phase state of SOA particles (which
 96 plays critical roles in various physical and chemical processes of aerosols)⁴⁷⁻⁵⁶ are
 97 elucidated and possible mechanisms are examined in light of predictions of a box
 98 model for this system. Initial studies of the ozonolysis of the much larger and
 99 complex biogenic alkene α -cedrene are also reported, and it is shown that the
 100 mechanism of particle formation for this sesquiterpene is different from that for
 101 *trans*-3-hexene. These results have important implications for modeling particle
 102 formation and growth in air from alkene ozonolysis.

103 Experimental

104 Apparatus

105 Ozonolysis experiments were conducted both in a flow reactor and in a static
106 chamber in the absence and presence of an OH or SCI scavenger at 295 ± 1 K.
107 Experiments on the effects of relative humidity (RH) were carried out in the
108 chamber.

109 **Flow reactor.** The major section of the reactor consisted of a 4.6 cm i.d. and 85 cm
110 long quartz tube. Two end caps were mated to the tube and sealed with O-rings.
111 Gas phase *trans*-3-hexene was generated by using an automated syringe pump
112 (Pump Systems Inc., model NE-1000) to inject the pure liquid (Sigma-Aldrich, >
113 99%) into 3.36 L min^{-1} dry air (Praxair, Ultra zero air). The air flow containing
114 *trans*-3-hexene was introduced concentrically into the reactor through the upstream
115 end cap. Ozone, produced by flowing O_2 (Praxair, Ultra High Purity, 99.993%) at
116 0.24 L min^{-1} through a pen-ray mercury lamp (model 11SC-2), was sent to the flow
117 reactor just downstream of the *trans*-3-hexene inlet through a perforated glass tube
118 in the radial direction. The O_3 concentration was measured using a UV-vis
119 spectrometer (Ocean Optics, HR4000). The total flow rate in the reactor was 3.6 L
120 min^{-1} , giving a residence time of 24 s. The typical initial concentrations of
121 *trans*-3-hexene and O_3 in the flow reactor were 12.5 ppm and 13 ppm, respectively.
122 In some experiments, ~ 6500 ppm of cyclohexane (Fisher Scientific, 99.99%) or
123 ~ 1800 ppm of chlorocyclohexane (Sigma-Aldrich, 99%) were added, using the same
124 method as for *trans*-3-hexene, to the flow reactor as a scavenger for OH formed from
125 ozonolysis.

126 At the outlet of the flow reactor, size distributions of SOA particles were measured
127 using a scanning mobility particle sizer (SMPS, TSI), which consists of an
128 electrostatic classifier (model 3080), a long differential mobility analyzer (DMA,
129 3081) and a condensation particle counter (model 3776). In addition, the
130 polydisperse particles exiting the flow reactor were collected on a 37-mm quartz
131 filter at a flow rate of 3.4 L min^{-1} for 60 min, with venting of the remaining flow at
132 0.2 L min^{-1} to the hood. Excellent collection efficiency ($> 99\%$) was obtained for
133 particles of all diameters by assaying for particles downstream of the filter using the

134 SMPS. After collection, the filters were immediately extracted with 2-mL
135 acetonitrile (Fisher Scientific, 99.9%) by sonicating for 12 min. The resulting
136 solutions were analyzed using an LCT Premier electrospray ionization time-of-flight
137 mass spectrometer (ESI-MS, Waters). In order to explore the size-dependence of
138 the composition, monodisperse particles of different sizes (50, 75, 80, 100, 150, and
139 200 nm) were selected using the DMA, and then either measured online using a high
140 resolution time-of-flight aerosol mass spectrometer (HR-ToF-AMS, Aerodyne) or
141 collected onto a quartz filter for offline ESI-MS measurements. It should be noted
142 that larger, multiply charged particles could also contribute in these size-selection
143 experiments due to their selection by electrical mobility.

144 To compare the particle formation mechanisms between small simple and large
145 complex alkenes, flow reactor experiments were also conducted to investigate
146 α -cedrene ozonolysis in the absence and presence of cyclohexane, using the same
147 experimental procedures as those for *trans*-3-hexene ozonolysis. The initial
148 concentrations of α -cedrene (Sigma-Aldrich, 98.0%), O₃ and cyclohexane (when
149 used) were 500 ppb, 16 ppm, and 262 ppm, respectively. The reaction time was 30
150 s. The polydisperse SOA particles formed in the reactor were collected for ESI-MS
151 analysis.

152 **Chamber.** Two types of chamber experiments were carried out: (i) ozonolysis of
153 *trans*-3-hexene in the absence and presence of formic acid or hydrochloric acid (HCl)
154 as an SCI scavenger in a 300 L Teflon chamber and (ii) ozonolysis of *trans*-3-hexene
155 at lower concentrations and different RH in a 450 L Teflon chamber. Formic acid
156 was added by injecting a known volume of liquid (Sigma-Aldrich, $\geq 95\%$) into the
157 chamber. The HCl solution (37% wt, J.T.Baker) was freeze-pump-thawed and the
158 headspace above the solution on warming expanded into a separate bulb, the
159 contents of which were flushed into the chamber. The vapor in the headspace
160 above such a solution at 293 K is comprised of $\sim 97\%$ HCl and $\sim 3\%$ water by
161 volume.⁵⁷ Water vapor was added by bubbling air through nanopure water into the
162 chamber. *trans*-3-Hexene was then added by injecting a defined volume of pure

163 liquid into the chamber. After 10 min to allow for the evaporation of
164 *trans*-3-hexene and mixing of the gases, O₃ produced by a commercial ozone
165 generator (Polymetrics, Model T-816) was added to the chamber to initiate the
166 reaction. Type (i) experiments were performed with initial *trans*-3-hexene and O₃
167 concentrations of 10 ppm each, and formic acid concentrations of 0-6 ppm and HCl
168 concentrations of 0-30 ppm. Type (ii) experiments were performed at an initial
169 *trans*-3-hexene concentration of 800 ppb and an O₃ concentration of 1.5 ppm in the
170 RH range of 0-80%, which was monitored using a humidity probe (Vaisala, HMT
171 234).

172 The size distribution of SOA particles formed in the chamber was measured using
173 SMPS. After an 18 min reaction, polydisperse particles were sampled onto a quartz
174 filter at a flow rate of 10 L min⁻¹. The filter was promptly extracted with 2-mL
175 acetonitrile by sonicating for 12 min, followed by ESI-MS analysis. In type (i)
176 experiments, SOA formed in the absence of formic acid was also impacted onto a
177 germanium (Ge) attenuated total reflectance (ATR) crystal using a custom designed
178 impactor⁵⁴ at a flow rate of 30 L min⁻¹ for 10 min for ATR-Fourier transform infrared
179 (ATR-FTIR) measurements.

180 In both the flow reactor and chamber experiments, a 10-cm monolith extruded
181 carbon denuder (NovacarbTM; Mast Carbon, Ltd.) was inserted in front of the filter to
182 remove the gas phase species before particle collection. Particle size distributions
183 obtained with and without the denuder show no significant difference. Blank
184 experiments were also performed with the same experimental procedures as the
185 ozonolysis experiments except that O₃ was not added to the flow reactor or the
186 chamber. Particle number concentrations were < 10 cm⁻³ in blank experiments.
187 No seed particles were added in any of these experiments.

188 SOA Characterization

189 **ESI-MS measurements.** Acetonitrile extracts of both SOA samples and blanks
190 were analyzed by ESI-MS. The ESI source was operated in positive ion mode under

191 optimum conditions as follows: capillary voltage 3.0 kV, desolvation gas flow 500 L
192 h^{-1} , and desolvation gas temperature 120 °C. Mass spectra were acquired over a
193 mass range of 200-1000 Da. Ions observed were primarily sodium adducts, $[\text{M} +$
194 $\text{Na}]^+$. Mass spectra of blanks, which contained peaks attributable mainly to the
195 impurities from the filter and acetonitrile solvent, were subtracted from the spectra of
196 SOA samples. Data analysis was performed using MassLynx software. Accurate
197 mass measurements were performed using polyethylene glycol, polyethylene glycol
198 monomethyl ether, or sodium formate as the mass calibration standards.

199 **AMS measurements.** An Aerodyne HR-ToF-AMS was used to measure the
200 chemical compositions of size-selected particles (50, 75, 100, 150, and 200 nm) in
201 the flow reactor experiments. Details of this instrument have been described
202 elsewhere.⁵⁸ Briefly, SOA particles sampled into the AMS (40-1000 nm) are
203 focused into a particle beam using an aerodynamic lens. The particles then travel
204 through a size-selecting vacuum chamber and are then vaporized at 600 °C. The
205 resulting vapors are then ionized by electron impact (70 eV) and analyzed with a ToF
206 mass analyzer. Elemental analysis was performed using the “Improved-Ambient”
207 method.⁵⁹ Measurements of effective density were made as a function of particle
208 diameter using the ratio of vacuum aerodynamic diameter to SMPS mobility
209 diameter, assuming the particles are spherical.⁶⁰

210 **ATR-FTIR measurements.** SOA particles from the chamber were impacted onto
211 a Ge ATR crystal that was transferred immediately into an ATR cell (volume $\sim 2 \text{ cm}^3$)
212 through which dry synthetic air was flowed at 30 ml min^{-1} . A Nicolet 6700 FTIR
213 spectrometer (Thermo Scientific) was used to record single beam spectra of the
214 crystal before and after the SOA was deposited, at a resolution of 4 cm^{-1} . One
215 hundred and twenty-eight scans were averaged for each spectrum. The absorbance
216 spectra of SOA on the crystal were then obtained as $\log_{10}(S_0/S_1)$ where S_0 and S_1
217 represent a background and a spectrum of interest, respectively.

218 **Results and Discussion**

219 Particle formation in the flow reactor with or without an OH scavenger

220 Figure 1 shows the ESI mass spectra of SOA particles formed from the ozonolysis of
221 *trans*-3-hexene in the absence and presence of cyclohexane or chlorocyclohexane for
222 a 24 s reaction time in the flow reactor. Ions corresponding to $[M + Na]^+$ are
223 observed across a mass range of 200-800 Da. In the mass spectrum obtained
224 without a scavenger (Fig. 1a), an obvious feature is the presence of an ion series
225 starting at m/z 305 with mass differences of m/z 74, suggesting the formation of
226 oligomers with a repeat unit that has the same mass as *trans*-3-hexene SCI
227 (CH_3CH_2CHOO). As discussed below, the species corresponding to m/z 305 is an
228 oligomer formed from a hexene alkyl peroxy radical and two SCI.

229 Table 1 shows the assignment of different oligomer series observed in the ESI
230 mass spectra. In the absence of a scavenger, OH radicals formed by ozonolysis
231 with a yield⁶¹ of ~47%, will react in air with *trans*-3-hexene, producing primarily
232 $CH_3CH_2CH(OH)CH(OO\cdot)CH_2CH_3$ (hereafter referred to as HE-RO₂, MW 133) as
233 the main RO₂ radicals. As observed in Fig. 1a, the ion series is consistent with the
234 oligomers formed from HE-RO₂ + n SCI + HO₂ where n represents the number of
235 SCI chain units. Hereafter, this oligomer series is termed as OLI-A. Accurate
236 mass determinations (Table 2) on selected OLI-A oligomers show very good
237 agreement with their expected elemental compositions. The ESI-MS results
238 presented here corroborate the oligomerization mechanism proposed by Sadezky and
239 co-workers,⁴³ however our data show an increased contribution from longer
240 oligomers, *i.e.*, $n > 5$, compared to the data reported by Sadezky *et al.*⁴³

241 In the presence of an OH scavenger, the reaction between the scavenger and OH
242 radicals contributes to the formation of a different RO₂ radical, which is also
243 expected to initiate oligomerization, thus resulting in the formation of a different
244 oligomer series. As shown in Fig. 1b and c, in addition to OLI-A, new oligomer
245 series starting from m/z 361 or m/z 321 were observed in the presence of
246 cyclohexane or chlorocyclohexane, respectively. These two new oligomer series
247 (hereafter termed as OLI-B and OLI-C) are attributed to the reactions of $CH-RO_2 + n$

248 SCI + HO₂ and Cl-RO₂ + *n* SCI + HO₂, where CH-RO₂ (MW 115) and Cl-RO₂ (MW
249 149) denote cyclohexyl peroxy and chlorocyclohexyl peroxy radicals produced by
250 the reaction of OH with cyclohexane and chlorocyclohexane, respectively.
251 Accurate mass measurements performed on selected *m/z* values were again in
252 excellent agreement with the predicted elemental compositions of oligomers for each
253 series, as reported in Table 2. As chlorine has two stable isotopes, ³⁵Cl and ³⁷Cl,
254 OLI-C was detected as a series of doublet peaks with intensity ratios equal to that of
255 the two isotopes, *i.e.*, 3:1.

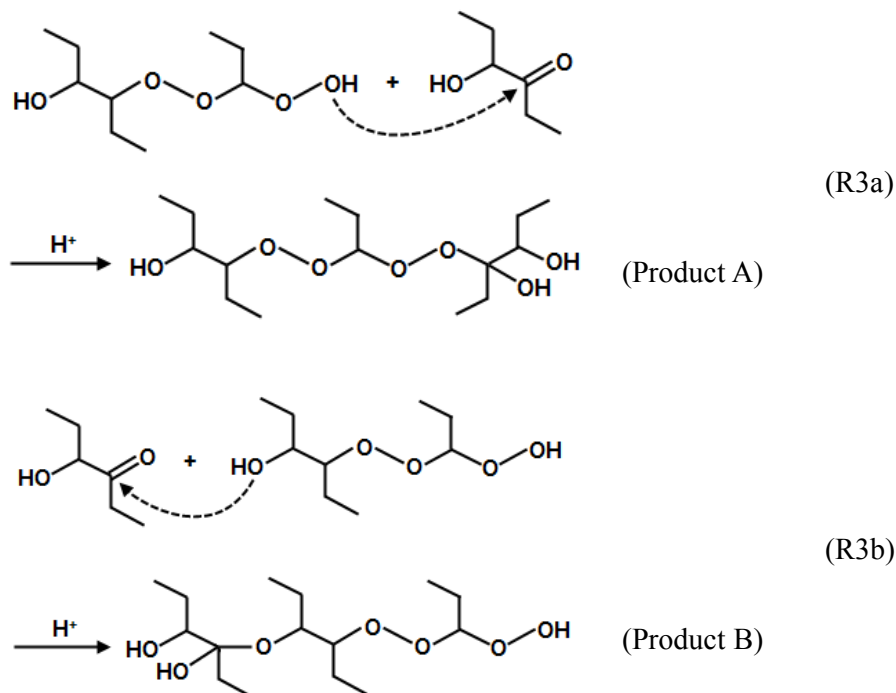
256 In the presence of cyclohexane or chlorocyclohexane, > 98% or > 90%,
257 respectively, of OH radicals should react with the scavenger based on the scavenger
258 concentrations used relative to *trans*-3-hexene. The formation of CH-RO₂ and
259 Cl-RO₂, therefore, would be expected to dominate over that of HE-RO₂.
260 Accordingly, the gas phase formation of OLI-B and OLI-C should prevail over
261 OLI-A. However, the OLI-A series is still significant in SOA particles formed in
262 the presence of a scavenger as seen in the ESI mass spectra (Fig. 1b and c). This
263 difference between gas phase formation and particle phase abundance of oligomers
264 is likely due, at least in part, to the different volatilities of the oligomer series. For
265 example, using the group-contribution method of Pankow and Asher,³⁶ the vapor
266 pressures of oligomers *n* = 2, 3, 4, 5 in OLI-A at 295 K are estimated to be 1.5×10^{-9}
267 atm, 3.2×10^{-11} atm, 6.8×10^{-13} atm, and 1.4×10^{-14} atm, respectively, over two
268 orders of magnitude lower than those of oligomers *n* = 2, 3, 4, 5 in OLI-B, which are
269 estimated to be 2.4×10^{-7} atm, 5.1×10^{-9} atm, 1.1×10^{-10} atm, and 2.3×10^{-12} atm at
270 295 K. Vapor pressures predicted using this method have an average uncertainty of
271 a factor of two. However, such uncertainty would not alter the calculated relative
272 vapor pressures of the oligomers. No values for halogenated subunits could be
273 found in this group-contribution method. However, the vapor pressure of
274 chlorocyclohexane has been reported to be 12 times lower than that of
275 cyclohexane,^{62,63} suggesting that OLI-C would be less volatile than OLI-B but still
276 more volatile than OLI-A. These calculations suggest that although more OLI-B or

277 OLI-C oligomers that incorporate CH-RO₂ or Cl-RO₂ are expected to be formed in
278 the presence of an OH scavenger, their higher volatilities lead to smaller
279 contributions to SOA. In addition, there may be steric hindrance to their formation
280 because of the presence of the 6-membered rings in CH-RO₂ and Cl-RO₂ that could
281 result in lower rate constants for CH-RO₂ + SCI and Cl-RO₂ + SCI. It is interesting
282 to note that when chlorocyclohexane is used, both the OLI-A and OLI-C series in
283 Fig. 1c contain shorter oligomers than in the absence of the scavenger (Fig. 1a).
284 This may be due to the consumption of SCI by some species (in addition to Cl-RO₂)
285 formed uniquely in the presence of chlorocyclohexane, which suppresses the growth
286 of the oligomer chain. It has been reported that the oxidation of chloroalkanes
287 forms HCl,^{64,65} and it is likely that HCl is also produced in the OH initiated oxidation
288 of chlorocyclohexane. If HCl reacts with SCI, as discussed below, it will inhibit the
289 formation of longer oligomers.

290 **Particle formation in the chamber with or without SCI scavenger**

291 Figure 2 shows the ESI mass spectra of SOA particles formed from the ozonolysis of
292 *trans*-3-hexene in the static chamber without or with formic acid as an SCI scavenger.
293 Compared to flow reactor experiments where smaller particles were observed (mean
294 size ~77 nm after a 24 s reaction), larger particles are measured in the chamber
295 experiments (mean size ~135 nm after an 18 min reaction). The ESI mass spectrum
296 in the absence of formic acid (Fig. 2a) is very similar to that obtained from the flow
297 reactor without OH scavenger (Fig. 1a), except for a shift in relative intensity of the
298 oligomers. The ESI mass spectra show that these chamber SOA particles at 18 min
299 have a higher contribution from oligomers $n \leq 3$ than the flow reactor SOA particle
300 at 24 s. This suggests a size-dependent growth mechanism for SOA particles. As
301 discussed later, it appears that oligomers $n \geq 4$ play a more important role in the
302 initial stages of particle formation, whereas oligomers $n \leq 3$ contribute mainly to
303 particle growth. It can be seen in Fig. 2b and c that the presence of formic acid,
304 which reacts with SCI,^{5,45,66-68} strongly suppresses the formation of longer oligomers,
305 confirming that SCI play a key role in oligomer formation.

306 It is worthwhile noting that there are two new peaks at m/z 347 and 421 in the
307 mass spectra with 6 ppm formic acid, which are attributed to products from
308 acid-catalyzed reactions in the particle phase. In order to verify this, we
309 investigated SOA formation from ozonolysis of *trans*-3-hexene in the presence of
310 gaseous hydrochloric acid (HCl). Figure 3 shows the ESI mass spectra of SOA
311 particles from ozonolysis of *trans*-3-hexene at different HCl concentrations.
312 Similar to the addition of formic acid (Fig. 2), the presence of HCl significantly
313 inhibits the formation of longer oligomers, suggesting that HCl can act as an SCI
314 scavenger. Notably, at higher HCl concentrations, a new oligomer series starting
315 at m/z 347 again with mass differences of 74 Da is formed in SOA. Hereafter, this
316 oligomer series is termed as OLI-D. Considering that the mass of OLI-D is 116 Da
317 higher relative to OLI-A and that this mass difference is the same as the molecular
318 weight of the primary OH oxidation product of *trans*-3-hexene,
319 $\text{CH}_3\text{CH}_2\text{CH}(\text{OH})\text{C}(\text{O})\text{CH}_2\text{CH}_3$ (hereafter referred to as HECAB), the OLI-D may be
320 either product A (in reaction R3a) or product B (in reaction R3b) formed by the
321 acid-catalyzed reaction of OLI-A with HECAB on the surface and/or in the bulk of
322 SOA particles (product A or B in reaction R3 would both be observed as $[\text{M} + \text{Na}]^+$
323 at m/z 347 in the mass spectra). Theoretical calculations have shown that the
324 formation of product B in the particle phase is not thermodynamically favorable.²¹
325 OLI-D, therefore, is more likely the peroxyhemiacetal product A. Accurate mass
326 measurements (Table 2) of selected OLI-D oligomers agree well with the expected
327 elemental composition for these peroxyhemiacetals. Formation of
328 peroxyhemiacetals has also been suggested in SOA from ozonolysis of
329 1-tetradecene,⁶⁹ α -pinene,^{16,23} and ethylene,⁴⁴ and photooxidation of dodecane⁷⁰ and
330 toluene.⁷¹



331 Figure 4 shows the number and mass concentrations, as well as the mean diameter
 332 of SOA particles formed from ozonolysis of *trans*-3-hexene at different formic acid
 333 concentrations. In addition to suppressing formation of longer oligomers, the
 334 presence of formic acid also significantly inhibited new particle formation while
 335 enhancing particle growth. This was also observed in experiments with HCl.
 336 These results suggest that long oligomers are the key nucleating species for particle
 337 formation, while condensable species (*e.g.*, short oligomers) are still being formed
 338 that can contribute to particle growth. Given the smaller number of particles that
 339 occur in the presence of formic acid, there should be more low MW condensable
 340 species available in the gas phase for each particle to grow to larger sizes.

341 Recently, Sakamoto *et al.*⁴⁴ observed the gas phase formation of oligomers
 342 containing SCI as the chain unit during ethylene ozonolysis and proposed a new
 343 oligomer formation mechanism (Reaction R2) involving sequential addition of SCI
 344 to organic hydroperoxides (ROOHs) instead of to RO₂ radicals. The
 345 hydroperoxides included 2-hydroxyethyl hydroperoxide (HOCH₂CH₂OOH)
 346 produced by OH oxidation of ethylene, and formyloxymethyl hydroperoxide

347 (HCOOCH₂OOH) formed from reaction of formic acid with SCI.

348 To test the contribution of this mechanism in the current system, oligomer
349 formation from ozonolysis of *trans*-3-hexene in the presence of formic acid was
350 simulated using a box model by assuming that oligomers are formed through ROOH
351 + *n* SCI (See details in the Supplementary Information).

352 Figure 5 shows the model-predicted gas phase formation of oligomers through
353 sequential addition of SCI to the two dominant organic hydroperoxides formed
354 during the ozonolysis, *i.e.*, *trans*-3-hexene derived hydroperoxide (HEOOH) from
355 HE-RO₂ + HO₂ reaction and 3-formyloxypopyl hydroperoxide (FPOOH) from
356 formic acid + SCI reaction. The predicted concentrations of oligomers from
357 FPOOH + *n* SCI are about 5 and 10 times higher than those from HEOOH + *n* SCI
358 in the presence of 2.1 and 6 ppm formic acid, respectively. Using a
359 group-contribution method,³⁶ the vapor pressures of oligomers *n* = 2, 3, 4 of FPOOH
360 + *n* SCI are estimated to be 1.2×10^{-7} atm, 2.5×10^{-9} atm, and 5.3×10^{-11} atm,
361 respectively, while the oligomers *n* = 2, 3, 4 of HEOOH + *n* SCI are approximately
362 1.5×10^{-9} atm, 3.2×10^{-11} atm, and 6.8×10^{-13} atm. Although the vapor pressure of
363 FPOOH + *n* SCI is about two orders of magnitude higher than HEOOH + *n* SCI, it is
364 comparable to that of HEOOH + (*n*-1) SCI. Given that the predicted gas phase
365 concentration of oligomers from FPOOH + *n* SCI is substantially higher than that for
366 HEOOH + (*n*-1) SCI (Fig. 5), the former oligomer series should have a greater
367 contribution to SOA formation than the latter. However, the ESI-MS spectra of
368 *trans*-3-hexene SOA in Fig. 2 show no evidence of oligomers from FPOOH + *n* SCI,
369 *e.g.*, no obvious peaks at *m/z* 291 (*n* = 2), 365 (*n* = 3), and 439 (*n* = 4). This
370 suggests that oligomers observed in the present study are not formed by ROOH + *n*
371 SCI, but rather through RO₂ + *n* SCI.

372 Particle formation at lower concentrations and different relative humidities

373 The reaction of SCI with water vapor is considered an important, sometimes
374 dominant, loss pathway for SCI in the atmosphere, with the extent depending on the

375 types of SCI.^{45,67,68,72-74} In order to evaluate the influence of water vapor on both
376 oligomer and new particle formation from ozonolysis, we conducted chamber
377 experiments over a wide range of relative humidities using 800 ppb *trans*-3-hexene
378 and 1.5 ppm O₃.

379 Figure 6 shows the ESI mass spectra of SOA particles formed from ozonolysis of
380 800 ppb *trans*-3-hexene at different RH. SOA particles formed at 800 ppb (Fig. 6a)
381 have a greater contribution from shorter oligomers compared to those formed at
382 higher concentrations (Fig. 2a). As the formation of SCI based oligomers involves
383 multistep reactions, higher reactant concentrations favor the formation of longer
384 oligomers. As observed in Fig. 6b and c, under humid conditions, the presence of
385 water significantly inhibits the formation of long oligomers ($n \geq 4$) by scavenging
386 SCI, but the formation of short oligomers is still evident even at 80% RH.
387 Interestingly, the peroxyhemiacetals (at m/z 347 and 421) observed in the
388 acid-catalyzed particle phase reaction of OLI-A with HECAB discussed above, are
389 also formed in SOA with their abundance increasing with rising RH. It has been
390 reported that under humid conditions Criegee intermediates can react with water
391 forming acids⁷³⁻⁷⁶ and/or hydroxyhydroperoxides (HHPs).⁷⁶⁻⁷⁹ HHPs can
392 subsequently decompose to either aldehydes/ketones and H₂O₂ or acids and
393 H₂O,^{77,78,80} with the decomposition being assisted by the presence of water vapor.^{79,80}
394 Therefore, as RH increases more acids will be produced,^{75,76,78} thus favoring the
395 formation of peroxyhemiacetals.

396 Figure 7 illustrates particle formation from ozonolysis as a function of RH.
397 Despite the suppressed production of key nucleating species (*i.e.*, oligomers $n \geq 4$),
398 particle number concentration increases unexpectedly with increasing RH.
399 Considering the reaction products derived from *trans*-3-hexene SCI and H₂O (*e.g.*,
400 1-hydroxypropyl hydroperoxide, HPOOH) are too volatile to act as nucleating
401 species, water may be involved in growing small clusters to detectable sizes. For
402 example, clusters from oligomeric products could H-bond to water via the –OH,
403 O–O and –OOH groups in the oligomer. Once a substantial number of new

404 particles are formed, they cannot grow to large sizes because of the lack of adequate
405 condensable material.

406 **Size-dependent composition and density of SOA**

407 As discussed above, the longer oligomers ($n \geq 4$) appear to be the key nucleating
408 species for particle formation, while the shorter oligomers mainly contribute to
409 particle growth. To test this hypothesis we conducted chemical composition
410 measurements of size-selected SOA particles formed in the flow reactor using
411 ESI-MS and HR-ToF-AMS. The results are shown in Fig. 8. The oligomer peaks
412 in the ESI mass spectra of size-selected particles were separated into three groups,
413 *i.e.*, $n = 3$, $n = 4-5$, and $n = 6-8$ according to the MW of the oligomers. Because the
414 $n = 2$ peak in the mass spectra has very low intensity and there is an interfering peak
415 in the blanks, it was not included in the analysis. Figure 8a shows the fraction of
416 oligomer intensity in each group to the total oligomer intensity, for the particles of
417 different sizes (80, 150 and 210 nm). Higher order oligomers ($n \geq 4$) comprise a
418 greater fraction of the total for smaller particles, while shorter oligomers ($n = 3$)
419 contribute relatively more to the larger particles.

420 AMS measurements provide complementary information to the ESI-MS data.
421 The harsh analysis conditions (vaporization at 600 °C and electron impact ionization
422 at 70 eV) in AMS lead to significant fragmentation of organic species. However,
423 high MW fragments (> 150 Da) are still observed in AMS spectra of size-selected
424 particles. Figure 8b shows the fraction of the total intensity for > 150 Da fragments
425 in the mass spectra as a function of the particle size from 50-200 nm. The fraction
426 of high MW fragments decreases significantly with increasing particle size,
427 indicating that smaller particles contain substantially more high MW compounds, *i.e.*,
428 oligomers (It is noted that larger, multiply charged particles can also contribute to
429 these size-selected samples with more highly charged particles mimicking smaller
430 ones; this would lead to an underestimate of the observed trend). Figure 8b also
431 shows the effective density of SOA as a function of particle size. The density
432 decreases from 1.12 g cm⁻³ for 50 nm particles to 0.82 g cm⁻³ for 200 nm particles.

433 Such a density gradient implies a change in composition as the particle grows.

434 Figure 8c shows size-dependent O/C and H/C ratios of the particles, obtained by
435 AMS. As the particles grow to larger sizes, the O/C ratio decreases from $0.57 \pm$
436 0.09 for 75 nm particles to 0.46 ± 0.02 for 200 nm particles. Correspondingly, the
437 H/C ratio increases from 1.90 ± 0.16 to 2.09 ± 0.02 . The O/C ratio of the smallest
438 measured particles (75 nm) is within experimental error of that of the observed
439 oligomers (*e.g.*, for $n = 4$, O/C = 0.61). This suggests that the growth of particles is
440 due to uptake of less oxygenated species (Again, the presence of larger, multiply
441 charged particles may lead to an underestimate in O/C ratios). A similar negative
442 correlation between the O/C ratio and particle size has also been shown for
443 α -pinene/O₃ SOA generated in a flow reactor by Tolocka *et al.*¹¹ It is worth noting
444 that the substantial decrease in density as a function of particle size is well correlated
445 with the decrease in the O/C ratio. This is consistent with previous measurements
446 of the density of organic aerosol, which showed that more oxidized particles have
447 higher density.^{81,82}

448 The size-dependent data support the hypothesis that SOA particles from
449 ozonolysis of *trans*-3-hexene are initially formed by nucleation of higher molecular
450 weight oligomers ($n \geq 4$) and then grow via condensation of shorter oligomers and
451 other less oxygenated, more volatile species.^{12,30,31,38,39}

452 **Phase state of SOA**

453 The phase of atmospheric particles (liquid/solid) plays a crucial role in various
454 physical and chemical processes of particles such as growth,^{49,50,52} aging,^{47,48,52,53} and
455 water uptake.^{48,51} In the present study, particle impaction/ATR-FTIR measurements
456 were performed to offer some insight into the phase/viscosity of *trans*-3-hexene SOA
457 since the impaction patterns on the Ge crystal have been shown to be an indicator of
458 phase.⁵⁴ For example, viscous liquid particles hit and stick to the crystal to form a
459 row of spots, whereas solid particles above a certain size bounce and can be
460 subsequently captured on the crystal, forming a disperse pattern dubbed "clouds".⁵⁴

461 Figure 9 shows a photograph of a typical impaction pattern of *trans*-3-hexene SOA
462 on a Ge ATR crystal. For comparison, the impaction pattern of SOA formed from
463 α -pinene ozonolysis obtained in a previous study⁵⁴ in our lab using the same
464 impactor is also shown. The *trans*-3-hexene SOA flows away from the centerline
465 that is the initial area of impact on the ATR crystal. This is in contrast to the
466 behavior of semi-solid α -pinene SOA which bounces but is subsequently captured on
467 the crystal, forming a more diffuse “cloud” pattern. The lack of “bounce”
468 establishes that *trans*-3-hexene SOA is less viscous than α -pinene SOA.

469 Figure 10a shows a typical ATR-FTIR spectrum of *trans*-3-hexene SOA collected
470 immediately following impaction. An obvious feature of the spectrum is the
471 presence of strong bands between 800-1200 cm^{-1} , likely because of the O–O and
472 C–O stretching vibrations in the C–O–O group.⁸³ The band attributable to C=O at
473 $\sim 1738 \text{ cm}^{-1}$ is weaker. This is consistent with the ESI-MS data, which suggest
474 *trans*-3-hexene SOA is mainly comprised of oligomers in which the repeat chain unit
475 contains a C–O–O group. Figure 10b is a difference spectrum showing the changes
476 in SOA upon exposure to a flow of clean dry air (30 mL min^{-1}) for 20 hours. More
477 volatile organic species in SOA may evaporate under such circumstances, leading to
478 a decrease in the peak intensities associated with those species. The ESI mass
479 spectra of SOA extracted from the crystal immediately following impaction and after
480 20 hours of air exposure showed that there is a preferential loss of oligomer $n = 1$
481 ($\sim 100\%$) and $n = 2$ ($\sim 65\%$) relative to $n \geq 3$ from the SOA on exposure to air.
482 However, as can be seen in Fig. 10b, the absorbance of many SOA peaks actually
483 increases. This is attributed to the spreading of SOA across the crystal under the air
484 flow. The depth of penetration of the IR beam at 1750 and 2950 cm^{-1} for SOA with
485 a refractive index of ~ 1.5 ^{84,85} on a Ge crystal is calculated to be 0.38 and 0.23 μm
486 respectively.⁸⁶ If the initial film thickness along and close to the centerline is much
487 larger than this, only a portion of the SOA is probed. As the film spreads out on the
488 crystal, more of the SOA is probed by the IR beam, leading to the increase in
489 absorbance. This supports the conclusion that *trans*-3-hexene SOA is less viscous

490 than α -pinene SOA. In the latter case negative peaks were observed in the
491 difference spectrum.³⁸

492 **Comparison to particle formation from α -cedrene**

493 Our study, together with earlier work by Sadezky *et al.*⁴³ suggests that formation of
494 oligomers involving $\text{RO}_2 + n \text{SCI}$ is a major contributor to SOA formation during the
495 ozonolysis of small alkenes. Given that substitution normally has significant
496 effects on the reactivity and chemistry of SCI,^{10,45,67,68} the mechanism of particle
497 formation from the ozonolysis may vary with the molecular size and structure of the
498 precursor alkenes. This poses the question as to how prevalent the $\text{RO}_2 + n \text{SCI}$
499 mechanism is in oligomer and SOA formation from ozonolysis of large and complex
500 alkenes such as terpenes and sesquiterpenes. In order to get some insight into this
501 question, we carried out flow reactor ozonolysis experiments with α -cedrene, a
502 sesquiterpene structurally similar to α -pinene, in the absence and presence of
503 cyclohexane. When the latter was present, it was at a sufficiently high
504 concentration to react with > 98% of OH radicals produced during ozonolysis.

505 Figure 11 shows typical ESI-MS spectra of SOA particles formed from ozonolysis
506 of α -cedrene in the absence and presence of cyclohexane. Formation of α -cedrene
507 derived monomers (m/z 240–350) and oligomers ($m/z > 420$) is evident both with
508 and without cyclohexane. In the presence of cyclohexane, two additional oligomer
509 patterns at m/z 350–410 and m/z 620–680 are formed in the SOA, likely resulting
510 from the combination of the oxidation products of cyclohexane and α -cedrene.
511 However, there are only minor contributions from peaks at m/z 391, 643, and 895,
512 which would correspond to the potential oligomeric products from sequential
513 addition of α -cedrene SCI to cyclohexane derived RO_2 (CH-RO_2) radicals. This is
514 despite the high yield (> 88%) of α -cedrene SCI from ozonolysis.⁸⁷ Thus, the RO_2
515 + $n \text{SCI}$ mechanism that dominates in the *trans*-3-hexene ozonolysis seems not to be
516 prevalent in SOA formation from α -cedrene oxidation. One potential reason is that
517 α -cedrene SCI may have a very low reactivity towards RO_2 radicals because of steric
518 effects attributable to the structure of this SCI. As a result, other reactions may be

519 more important in particle formation.^{87,88} For example, it has been suggested
520 recently that highly oxidized ELVOC formed by ozonolysis of α -pinene play a
521 critical role in the nucleation and growth of SOA particles.^{29,30,32,35} Given that
522 α -cedrene is similar to α -pinene in structure, α -cedrene ozonolysis may also be able
523 to produce such ELVOC.

524 Recently, Yao and coworkers have shown that during the ozonolysis of α -cedrene,
525 the addition of an SCI scavenger, acetic acid, led to fewer particles but higher SOA
526 mass yield.⁸⁷ Similar SCI scavenger effects have been observed for ozonolysis of
527 β -pinene²⁰ and β -caryophyllene⁸⁹ in the presence of formic acid. In contrast, in the
528 present study with *trans*-3-hexene, while the presence of formic acid inhibits new
529 particle formation, it also strongly decreases SOA mass loading (Fig. 4). One
530 explanation for this difference is that the products of reactions between large terpene
531 SCI and the scavenger have low enough volatility to contribute significantly to
532 particle growth, leading to a high SOA mass,^{20,87,89} whereas the 3-formyloxypropyl
533 hydroperoxide (FPOOH), produced by the reaction of small *trans*-3-hexene SCI with
534 formic acid, is too volatile (the vapor pressure is estimated to be 2.6×10^{-4} atm at
535 295 K using a group-contribution method)³⁶ to significantly contribute to particle
536 growth.

537 **Conclusions and Atmospheric Implications**

538 These studies show that particle formation in the *trans*-3-hexene ozonolysis is
539 consistent with the sequential addition of SCI to RO₂ radicals as previously proposed
540 by Sadezky *et al.*⁴³ Size-dependent oligomeric and elemental composition of SOA
541 particles show that longer oligomers play a key role in initial particle formation and
542 that subsequent growth occurs by condensation of shorter oligomers and other less
543 oxygenated, more volatile products. In addition, impaction/ATR-FTIR
544 measurements show that *trans*-3-hexene SOA is less viscous than α -pinene SOA.

545 However, the results of the α -cedrene ozonolysis experiments suggest that such
546 oligomerization reactions may not play a major role in particle formation from large

547 alkenes such as terpenes and sesquiterpenes. In these cases, it may be that the
548 recently proposed ELVOC formation involving a series of intramolecular H
549 abstractions/O₂ additions via RO₂ radicals^{30,32,34} from ozonolysis is the major particle
550 formation pathway.³⁰ Compared to terpene-RO₂ (*e.g.*, from α -pinene) where the
551 structure favors the intramolecular H abstractions to produce ELVOC, the RO₂
552 radicals produced during ozonolysis of small alkenes may be too short to go through
553 that pathway.

554 Considering that small alkenes make up a substantial fraction of VOCs in the
555 atmosphere,^{90,91} oligomer formation involving addition of their SCI to RO₂ radicals
556 can have implications for atmospheric particle formation. However, in the
557 atmosphere, such oligomer formation is expected to be strongly influenced by other
558 gas phase species that can competitively react with alkene RO₂ and SCI. For
559 example, RO₂ radicals can also react with NO, HO₂, and other RO₂ in the
560 atmosphere, with the relative importance depending particularly on the NO
561 concentration.^{5,45,92} Vereecken *et al.*⁴⁵ suggested that in a tropical forest area (*e.g.*,
562 Suriname) the RO₂ + SCI reactions accounted for only 0.1% of RO₂ losses,
563 assuming a rate constant of $5 \times 10^{-12} \text{ cm}^3 \text{ molecules}^{-1} \text{ s}^{-1}$. However, they point out
564 that this rate constant was a conservative estimate and it could be on the order of
565 $10^{-11} \text{ cm}^3 \text{ molecules}^{-1} \text{ s}^{-1}$. In addition, SCI react with a number of other atmospheric
566 species, *e.g.*, H₂O, SO₂, NO₂, carboxylic acids, as well as carbonyl and hydroxyl
567 compounds.^{5,45,66-68,72,93-95} Bimolecular reactions with these scavengers, in
568 particular H₂O, have been suggested to be the dominant loss pathway of some SCIs
569 in the atmosphere.^{45,67,72} However, in the present study, water vapor was shown to
570 increase new particle formation while decreasing the total mass.

571 Although the RO₂ + SCI reactions may not be important as a major loss process
572 for RO₂ and SCI in the atmosphere, these reactions produce high molecular weight
573 highly oxidized oligomeric products that have sufficiently low volatilities to form
574 SOA. Moreover, in some circumstances scavenging of SCI may not necessarily
575 suppress particle formation. For example, in the presence of SO₂, the reactions

576 between SCI and SO₂ can lead to the formation of H₂SO₄,^{5,74,93,96,97} an important
577 nucleation precursor.^{98,99}

578 A quantitative evaluation of the atmospheric importance of RO₂ + SCI reactions is
579 not possible at the moment because of the large uncertainties in the rate constants for
580 bimolecular reactions of SCI,^{45,67} especially those of RO₂ + SCI reactions for which
581 experimental data are not available. Therefore, further studies of the bimolecular
582 chemistry of SCI are needed in order to better understand the RO₂ + SCI chemistry
583 and its impacts on SOA formation in the atmosphere.

584 **Acknowledgements**

585 The authors gratefully thank National Science Foundation (Grants # 0909227 and
586 1207112) for support of this work, and the NSF Major Research Instrumentation
587 (MRI) program (Grant # 0923323 and 1337080) for HR-ToF-AMS.
588

589 Table 1 Summary of oligomer formation from the ozonolysis of *trans*-3-hexene in
 590 the flow reactor in the absence and presence of an OH scavenger.

Scavenger	Oligomer									
	series	Mechanisms	n=1 ^a	n=2	n=3	n=4	n=5	n=6	n=7	n=8
None	OLI-A	HE-RO ₂ +SCI	(231) ^b	305	379	453	527	601	675	749
cyclohexane	OLI-B	CH-RO ₂ +SCI	(213)	(287) ^b	361	435	509	583		
chlorocyclohexane	OLI-C	³⁵ Cl-RO ₂ +SCI	(247)	321	395	469				
		³⁷ Cl-RO ₂ +SCI	(249)	323	397	471				

591 ^a The values for the oligomer series correspond to the mass to charge (*m/z*) ratios of
 592 the [M + Na]⁺ ions in the ESI-MS spectra; *n* represents the number of chain units in
 593 the oligomers.

594 ^b These oligomers were not observed in the ESI-MS spectra probably because of
 595 their relatively higher volatility and thus lower contributions to the flow reactor SOA.

596 Table 2 Accurate mass data and elemental composition for different oligomer
 597 series formed in *trans*-3-hexene ozonolysis with and without OH or SCI scavengers.

Oligomer series	No. of chain units	Observed accurate mass (Da)	Elemental composition	Calculated exact mass (Da)	Absolute mass error (mDa)	Relative mass error (ppm)
OLI-A	n=3	379.1950	C ₁₅ H ₃₂ O ₉ Na	379.1944	0.6	1.6
	n=4	453.2295	C ₁₈ H ₃₈ O ₁₁ Na	453.2312	-1.7	-3.7
	n=5	527.2675	C ₂₁ H ₄₄ O ₁₃ Na	527.2680	-0.5	-0.9
OLI-B	n=3	361.1821	C ₁₅ H ₃₀ O ₈ Na	361.1838	-1.7	-4.8
	n=4	435.2189	C ₁₈ H ₃₆ O ₁₀ Na	435.2206	-1.7	-3.9
OLI-C	n=2	321.1095	C ₁₂ H ₂₃ O ₆ ³⁵ ClNa	321.1081	1.4	4.4
	n=3	395.1458	C ₁₅ H ₂₉ O ₈ ³⁵ ClNa	395.1449	0.9	2.4
OLI-D	n=1	347.2057	C ₁₅ H ₃₂ O ₇ Na	347.2046	1.1	3.2
	n=2	421.2400	C ₁₈ H ₃₈ O ₉ Na	421.2414	-1.4	-3.2

598

599 **References**

- 600 1 M. Hallquist, J. C. Wenger, U. Baltensperger, Y. Rudich, D. Simpson, M. Claeys,
601 J. Dommen, N. M. Donahue, C. George, A. H. Goldstein, J. F. Hamilton, H.
602 Herrmann, T. Hoffmann, Y. Iinuma, M. Jang, M. E. Jenkin, J. L. Jimenez, A.
603 Kiendler-Scharr, W. Maenhaut, G. McFiggans, T. F. Mentel, A. Monod, A. S. H.
604 Prevot, J. H. Seinfeld, J. D. Surratt, R. Szmigielski and J. Wildt, *Atmos. Chem. Phys.*,
605 2009, **9**, 5155-5236.
- 606 2 J. L. Jimenez, M. R. Canagaratna, N. M. Donahue, A. S. H. Prevot, Q. Zhang, J.
607 H. Kroll, P. F. DeCarlo, J. D. Allan, H. Coe, N. L. Ng, A. C. Aiken, K. S. Docherty, I.
608 M. Ulbrich, A. P. Grieshop, A. L. Robinson, J. Duplissy, J. D. Smith, K. R. Wilson, V.
609 A. Lanz, C. Hueglin, Y. L. Sun, J. Tian, A. Laaksonen, T. Raatikainen, J. Rautiainen,
610 P. Vaattovaara, M. Ehn, M. Kulmala, J. M. Tomlinson, D. R. Collins, M. J. Cubison,
611 E. J. Dunlea, J. A. Huffman, T. B. Onasch, M. R. Alfarra, P. I. Williams, K. Bower, Y.
612 Kondo, J. Schneider, F. Drewnick, S. Borrmann, S. Weimer, K. Demerjian, D.
613 Salcedo, L. Cottrell, R. Griffin, A. Takami, T. Miyoshi, S. Hatakeyama, A. Shimono,
614 J. Y. Sun, Y. M. Zhang, K. Dzepina, J. R. Kimmel, D. Sueper, J. T. Jayne, S. C.
615 Herndon, A. M. Trimborn, L. R. Williams, E. C. Wood, A. M. Middlebrook, C. E.
616 Kolb, U. Baltensperger and D. R. Worsnop, *Science*, 2009, **326**, 1525-1529.
- 617 3 M. Kanakidou, J. H. Seinfeld, S. N. Pandis, I. Barnes, F. J. Dentener, M. C.
618 Facchini, R. Van Dingenen, B. Ervens, A. Nenes, C. J. Nielsen, E. Swietlicki, J. P.
619 Putaud, Y. Balkanski, S. Fuzzi, J. Horth, G. K. Moortgat, R. Winterhalter, C. E. L.
620 Myhre, K. Tsigaridis, E. Vignati, E. G. Stephanou and J. Wilson, *Atmos. Chem. Phys.*,
621 2005, **5**, 1053-1123.
- 622 4 N. L. Ng, M. R. Canagaratna, Q. Zhang, J. L. Jimenez, J. Tian, I. M. Ulbrich, J.
623 H. Kroll, K. S. Docherty, P. S. Chhabra, R. Bahreini, S. M. Murphy, J. H. Seinfeld, L.
624 Hildebrandt, N. M. Donahue, P. F. DeCarlo, V. A. Lanz, A. S. H. Prevot, E. Dinar, Y.
625 Rudich and D. R. Worsnop, *Atmos. Chem. Phys.*, 2010, **10**, 4625-4641.
- 626 5 B. J. Finlayson-Pitts and J. N. Pitts, *Chemistry of the upper and lower*
627 *atmosphere: theory, experiments, and applications*, Academic Press, San Diego,
628 2000.
- 629 6 J. H. Seinfeld and S. N. Pandis, *Atmospheric Chemistry and Physics: from air*
630 *pollution to climate change*, J. Wiley, Hoboken, N.J., 2006.
- 631 7 J. H. Kroll and J. H. Seinfeld, *Atmos. Environ.*, 2008, **42**, 3593-3624.
- 632 8 P. J. Ziemann and R. Atkinson, *Chem. Soc. Rev.*, 2012, **41**, 6582-6605.
- 633 9 IPCC, *Summary for Policymakers. In: Climate Change 2013: The Physical*
634 *Science Basis. Contribution of Working Group I to the Fifth Assessment Report of the*
635 *Intergovernmental Panel on Climate Change [Stocker, T.F., D. Qin, G.-K. Plattner, M.*
636 *Tignor, S.K. Allen, J. Boschung, A. Nauels, Y. Xia, V. Bex and P.M. Midgley (eds.)].*
637 *Cambridge University Press, Cambridge, United Kingdom and New York, NY, USA.,*
638 2013.
- 639 10 D. Johnson and G. Marston, *Chem. Soc. Rev.*, 2008, **37**, 699-716.
- 640 11 A. Lee, A. H. Goldstein, M. D. Keywood, S. Gao, V. Varutbangkul, R. Bahreini,
641 N. L. Ng, R. C. Flagan and J. H. Seinfeld, *J. Geophys. Res.*, 2006, **111**, DOI:

- 642 10.1029/2005JD006437.
- 643 12 M. P. Tolocka, K. J. Heaton, M. A. Dreyfus, S. Y. Wang, C. A. Zordan, T. D.
644 Saul and M. V. Johnston, *Environ. Sci. Technol.*, 2006, **40**, 1843-1848.
- 645 13 M. P. Tolocka, M. Jang, J. M. Ginter, F. J. Cox, R. M. Kamens and M. V.
646 Johnston, *Environ. Sci. Technol.*, 2004, **38**, 1428-1434.
- 647 14 W. A. Hall and M. V. Johnston, *Aerosol Sci. Technol.*, 2011, **45**, 37-45.
- 648 15 K. J. Heaton, M. A. Dreyfus, S. Wang and M. V. Johnston, *Environ. Sci. Technol.*,
649 2007, **41**, 6129-6136.
- 650 16 W. A. Hall and M. V. Johnston, *J. Am. Soc. Mass Spectrom.*, 2012, **23**,
651 1097-1108.
- 652 17 K. Kristensen, T. Cui, H. Zhang, A. Gold, M. Glasius and J. D. Surratt, *Atmos.*
653 *Chem. Phys.*, 2014, **14**, 4201-4218.
- 654 18 B. Witkowski and T. Gierczak, *Atmos. Environ.*, 2014, **95**, 59-70.
- 655 19 S. Lee and R. M. Kamens, *Atmos. Environ.*, 2005, **39**, 6822-6832.
- 656 20 B. Bonn, G. Schuster and G. K. Moortgat, *J. Phys. Chem. A*, 2002, **106**,
657 2869-2881.
- 658 21 J. W. DePalma, A. J. Horan, W. A. Hall and M. V. Johnston, *Phys. Chem. Chem.*
659 *Phys.*, 2013, **15**, 6935-6944.
- 660 22 F. Yasmeen, R. Vermeylen, R. Szmigielski, Y. Iinuma, O. Boge, H. Herrmann, W.
661 Maenhaut and M. Claeys, *Atmos. Chem. Phys.*, 2010, **10**, 9383-9392.
- 662 23 L. Muller, M. C. Reinnig, H. Hayen and T. Hoffmann, *Rapid Commun. Mass*
663 *Spectrom.*, 2009, **23**, 971-979.
- 664 24 K. S. Docherty, W. Wu, Y. B. Lim and P. J. Ziemann, *Environ. Sci. Technol.*,
665 2005, **39**, 4049-4059.
- 666 25 P. J. Ziemann, *J. Phys. Chem. A*, 2003, **107**, 2048-2060.
- 667 26 M. Camredon, J. F. Hamilton, M. S. Alam, K. P. Wyche, T. Carr, I. R. White, P.
668 S. Monks, A. R. Rickard and W. J. Bloss, *Atmos. Chem. Phys.*, 2010, **10**, 2893-2917.
- 669 27 M. Claeys, Y. Iinuma, R. Szmigielski, J. D. Surratt, F. Blockhuys, C. Van
670 Alsenoy, O. Boge, B. Sierau, Y. Gomez-Gonzalez, R. Vermeylen, P. Van der Veken,
671 M. Shahgholi, A. W. H. Chan, H. Herrmann, J. H. Seinfeld and W. Maenhaut,
672 *Environ. Sci. Technol.*, 2009, **43**, 6976-6982.
- 673 28 T. Hoffmann, R. Bandur, U. Marggraf and M. Linscheid, *J. Geophys. Res.*, 1998,
674 **103**, 25569-25578.
- 675 29 M. Ehn, E. Kleist, H. Junninen, T. Petaja, G. Lonn, S. Schobesberger, M. Dal
676 Maso, A. Trimborn, M. Kulmala, D. R. Worsnop, A. Wahner, J. Wildt and T. F.
677 Mentel, *Atmos. Chem. Phys.*, 2012, **12**, 5113-5127.
- 678 30 M. Ehn, J. A. Thornton, E. Kleist, M. Sipila, H. Junninen, I. Pullinen, M.
679 Springer, F. Rubach, R. Tillmann, B. Lee, F. Lopez-Hilfiker, S. Andres, I. H. Acir, M.
680 Rissanen, T. Jokinen, S. Schobesberger, J. Kangasluoma, J. Kontkanen, T. Nieminen,
681 T. Kurten, L. B. Nielsen, S. Jorgensen, H. G. Kjaergaard, M. Canagaratna, M. Dal
682 Maso, T. Berndt, T. Petaja, A. Wahner, V. M. Kerminen, M. Kulmala, D. R. Worsnop,
683 J. Wildt and T. F. Mentel, *Nature*, 2014, **506**, 476-479.
- 684 31 J. Zhao, J. Ortega, M. Chen, P. H. McMurry and J. N. Smith, *Atmos. Chem.*
685 *Phys.*, 2013, **13**, 7631-7644.

- 686 32 M. P. Rissanen, T. Kurten, M. Sipila, J. A. Thornton, O. Kausiala, O. Garmash,
687 H. G. Kjaergaard, T. Petaja, D. R. Worsnop, M. Ehn, and M. Kulmala, *J. Phys. Chem.*
688 *A*, 2015, **119**, DOI: 10.1021/jp510966g.
- 689 33 L. Vereecken, J. F. Muller and J. Peeters, *Phys. Chem. Chem. Phys.*, 2007, **9**,
690 5241-5248.
- 691 34 J. D. Crounse, L. B. Nielsen, S. Jorgensen, H. G. Kjaergaard and P. O. Wennberg,
692 *J. Phys. Chem. Lett.*, 2013, **4**, 3513-3520.
- 693 35 M. P. Rissanen, T. Kurten, M. Sipila, J. A. Thornton, J. Kangasluoma, N. Samela,
694 H. Junninen, S. Jorgensen, S. Schallhart, M. K. Kajos, R. Taipale, M. Springer, T. F.
695 Mentel, T. Ruuskanen, T. Petaja, D. R. Worsnop, H. G. Kjaergaard and M. Ehn, *J.*
696 *Am. Chem. Soc.*, 2014, **136**, 15596-15606.
- 697 36 J. F. Pankow and W. E. Asher, *Atmos. Chem. Phys.*, 2008, **8**, 2773-2796.
- 698 37 B. Bonn and G. K. Moortgat, *Geophys. Res. Lett.*, 2003, **30**,
699 DOI: 10.1029/2003GL017000.
- 700 38 C. Kidd, V. Perraud and B. J. Finlayson-Pitts, *Phys. Chem. Chem. Phys.*, 2014,
701 **16**, 22706-22716.
- 702 39 P. M. Winkler, J. Ortega, T. Karl, L. Cappellin, H. R. Friedli, K. Barsanti, P. H.
703 McMurry and J. N. Smith, *Geophys. Res. Lett.*, 2012, **39**, DOI:
704 10.1029/2012GL053253.
- 705 40 T. B. Nguyen, A. P. Bateman, D. L. Bones, S. A. Nizkorodov, J. Laskin and A.
706 Laskin, *Atmos. Environ.*, 2010, **44**, 1032-1042.
- 707 41 S. Inomata, K. Sato, J. Hirokawa, Y. Sakamoto, H. Tanimoto, M. Okumura, S.
708 Tohno and T. Imamura, *Atmos. Environ.*, 2014, **97**, 397-405.
- 709 42 A. Sadezky, P. Chaimbault, A. Mellouki, A. Rompp, R. Winterhalter, G. Le Bras
710 and G. K. Moortgat, *Atmos. Chem. Phys.*, 2006, **6**, 5009-5024.
- 711 43 A. Sadezky, R. Winterhalter, B. Kanawati, A. Rompp, B. Spengler, A. Mellouki,
712 G. L. Bras, P. Chaimbault and G. K. Moortgat, *Atmos. Chem. Phys.*, 2008, **8**,
713 2667-2699.
- 714 44 Y. Sakamoto, S. Inomata and J. Hirokawa, *J. Phys. Chem. A*, 2013, **117**,
715 12912-12921.
- 716 45 L. Vereecken, H. Harder and A. Novelli, *Phys. Chem. Chem. Phys.*, 2012, **14**,
717 14682-14695.
- 718 46 J. M. Anglada, S. Olivella and A. Sole, *Phys. Chem. Chem. Phys.*, 2013, **15**,
719 18921-18933.
- 720 47 M. Shiraiwa, M. Ammann, T. Koop and U. Poschl, *Proc. Natl. Acad. Sci. U. S.*
721 *A.*, 2011, **108**, 11003-11008.
- 722 48 T. Koop, J. Bookhold, M. Shiraiwa and U. Poschl, *Phys. Chem. Chem. Phys.*,
723 2011, **13**, 19238-19255.
- 724 49 M. Shiraiwa and J. H. Seinfeld, *Geophys. Res. Lett.*, 2012, **39**, DOI:
725 10.1029/2012GL054008.
- 726 50 V. Perraud, E. A. Bruns, M. J. Ezell, S. N. Johnson, Y. Yu, M. L. Alexander, A.
727 Zelenyuk, D. Imre, W. L. Chang, D. Dabdub, J. F. Pankow and B. J. Finlayson-Pitts,
728 *Proc. Natl. Acad. Sci. U. S. A.*, 2012, **109**, 2836-2841.
- 729 51 D. L. Bones, J. P. Reid, D. M. Lienhard and U. K. Krieger, *Proc. Natl. Acad. Sci.*

- 730 *U. S. A.*, 2012, **109**, 11613-11618.
- 731 52 L. Renbaum-Wolff, J. W. Grayson, A. P. Bateman, M. Kuwata, M. Sellier, B. J.
- 732 Murray, J. E. Shilling, S. T. Martin and A. K. Bertram, *Proc. Natl. Acad. Sci. U. S. A.*,
- 733 2013, **110**, 8014-8019.
- 734 53 I. J. George and J. P. D. Abbatt, *Nature Chem.*, 2010, **2**, 713-722.
- 735 54 C. Kidd, V. Perraud, L. M. Wingen and B. J. Finlayson-Pitts, *Proc. Natl. Acad.*
- 736 *Sci. U. S. A.*, 2014, **111**, 7552-7557.
- 737 55 T. D. Vaden, D. Imre, J. Beranek, M. Shrivastava and A. Zelenyuk, *Proc. Natl.*
- 738 *Acad. Sci. U. S. A.*, 2011, **108**, 2190-2195.
- 739 56 H. Lignell, M. L. Hinks and S. A. Nizkorodov, *Proc. Natl. Acad. Sci. U. S. A.*,
- 740 2014, **111**, 13780-13785.
- 741 57 J. J. Fritz and C. R. Fuget, *Ind. Eng. Chem.*, 1956, **1**, 10-12.
- 742 58 P. F. DeCarlo, J. R. Kimmel, A. Trimborn, M. J. Northway, J. T. Jayne, A. C.
- 743 Aiken, M. Gonin, K. Fuhrer, T. Horvath, K. S. Docherty, D. R. Worsnop and J. L.
- 744 Jimenez, *Anal. Chem.*, 2006, **78**, 8281-8289.
- 745 59 M. R. Canagaratna, J. L. Jimenez, J. H. Kroll, Q. Chen, S. H. Kessler, P. Massoli,
- 746 L. Hildebrandt Ruiz, E. Fortner, L. R. Williams, K. R. Wilson, J. D. Surratt, N. M.
- 747 Donahue, J. T. Jayne, D. R. Worsnop, *Atmos. Chem. Phys.*, 2015, **15**, 253-272.
- 748 60 P. F. DeCarlo, J. G. Slowik, D. R. Worsnop, P. Davidovits and J. L. Jimenez,
- 749 *Aerosol Sci. Technol.*, 2004, **38**, 1185-1205.
- 750 61 J. D. Fenske, A. S. Hasson, S. E. Paulson, K. T. Kuwata, A. Ho and K. N. Houk,
- 751 *J. Phys. Chem. A*, 2000, **104**, 7821-7833.
- 752 62 A. J. B. Cruickshank and A. J. B. Cutler, *J. Chem. Eng. Data*, 1967, **12**, 326-329.
- 753 63 S. Sarraute, I. Mokbel, M. F. C. Gomes, V. Majer and J. Jose, *Atmos. Environ.*,
- 754 2008, **42**, 4724-4734.
- 755 64 G. Koltzenburg, G. Behrens and D. Schultefrohlinde, *J. Am. Chem. Soc.*, 1982,
- 756 **104**, 7311-7312.
- 757 65 J. J. Orlando and G. S. Tyndall, *J. Phys. Chem. A*, 2002, **106**, 312-319.
- 758 66 O. Welz, A. J. Eskola, L. Sheps, B. Rotavera, J. D. Savee, A. M. Scheer, D. L.
- 759 Osborn, D. Lowe, A. M. Booth, P. Xiao, M. A. H. Khan, C. J. Percival, D. E.
- 760 Shallcross and C. A. Taatjes, *Angew. Chem., Int. Ed.*, 2014, **53**, 4547-4550.
- 761 67 C. A. Taatjes, D. E. Shallcross and C. J. Percival, *Phys. Chem. Chem. Phys.*,
- 762 2014, **16**, 1704-1718.
- 763 68 L. Vereecken and J. S. Francisco, *Chem. Soc. Rev.*, 2012, **41**, 6259-6293.
- 764 69 H. J. Tobias and P. J. Ziemann, *Environ. Sci. Technol.*, 2000, **34**, 2105-2115.
- 765 70 M. Shiraiwa, L. D. Yee, K. A. Schilling, C. L. Loza, J. S. Craven, A. Zuend, P. J.
- 766 Ziemann and J. H. Seinfeld, *Proc. Natl. Acad. Sci. U. S. A.*, 2013, **110**, 11746-11750.
- 767 71 K. Sato, S. Hatakeyama and T. Imamura, *J. Phys. Chem. A*, 2007, **111**,
- 768 9796-9808.
- 769 72 C. A. Taatjes, O. Welz, A. J. Eskola, J. D. Savee, A. M. Scheer, D. E. Shallcross,
- 770 B. Rotavera, E. P. F. Lee, J. M. Dyke, D. K. W. Mok, D. L. Osborn and C. J. Percival,
- 771 *Science*, 2013, **340**, 177-180.
- 772 73 S. Hatakeyama, H. Bandow, M. Okuda and H. Akimoto, *J. Phys. Chem.*, 1981,
- 773 **85**, 2249-2254.

- 774 74 S. Hatakeyama and H. Akimoto, *Res. Chem. Intermed.*, 1994, **20**, 503-524.
775 75 O. Horie, P. Neeb, S. Limbach and G. K. Moortgat, *Geophys. Res. Lett.*, 1994,
776 **21**, 1523-1526.
777 76 K. E. Leather, M. R. McGillen, M. C. Cooke, S. R. Utembe, A. T. Archibald, M.
778 E. Jenkin, R. G. Derwent, D. E. Shallcross and C. J. Percival, *Atmos. Chem. Phys.*,
779 2012, **12**, 469-479.
780 77 S. Gab, E. Hellpointner, W. V. Turner and F. Korte, *Nature*, 1985, **316**, 535-536.
781 78 P. Neeb, F. Sauer, O. Horie and G. K. Moortgat, *Atmos. Environ.*, 1997, **31**,
782 1417-1423.
783 79 D. Huang, Z. M. Chen, Y. Zhao and H. Liang, *Atmos. Chem. Phys.*, 2013, **13**,
784 5671-5683.
785 80 P. Aplincourt and J. M. Anglada, *J. Phys. Chem. A*, 2003, **107**, 5812-5820.
786 81 J. E. Shilling, Q. Chen, S. M. King, T. Rosenoern, J. H. Kroll, D. R. Worsnop, P.
787 F. DeCarlo, A. C. Aiken, D. Sueper, J. L. Jimenez and S. T. Martin, *Atmos. Chem.*
788 *Phys.*, 2009, **9**, 771-782.
789 82 J. H. Kroll, J. D. Smith, D. L. Che, S. H. Kessler, D. R. Worsnop and K. R.
790 Wilson, *Phys. Chem. Chem. Phys.*, 2009, **11**, 8005-8014.
791 83 G. Socrates, *Infrared and Raman characteristic group frequencies: tables and*
792 *charts*, Wiley, Chichester; New York, 2001.
793 84 H. Kim, B. Barkey and S. E. Paulson, *J. Geophys. Res.*, 2010, **115**,
794 DOI: 10.1029/2010JD014549.
795 85 A. T. Lambe, C. D. Cappa, P. Massoli, T. B. Onasch, S. D. Forestieri, A. T.
796 Martin, M. J. Cummings, D. R. Croasdale, W. H. Brune, D. R. Worsnop and P.
797 Davidovits, *Environ. Sci. Technol.*, 2013, **47**, 6349-6357.
798 86 N. J. Harrick, *Internal reflection spectroscopy*, Interscience Publishers, New
799 York, 1967.
800 87 L. Yao, Y. Ma, L. Wang, J. Zheng, A. Khalizov, M. D. Chen, Y. Y. Zhou, L. Qi
801 and F. P. Cui, *Atmos. Environ.*, 2014, **94**, 448-457.
802 88 M. Jaoui, K. G. Sexton and R. M. Kamens, *Atmos. Environ.*, 2004, **38**,
803 2709-2725.
804 89 R. Winterhalter, F. Herrmann, B. Kanawati, T. L. Nguyen, J. Peeters, L.
805 Vereecken and G. K. Moortgat, *Phys. Chem. Chem. Phys.*, 2009, **11**, 4152-4172.
806 90 B. Barletta, S. Meinardi, F. S. Rowland, C. Y. Chan, X. M. Wang, S. C. Zou, L.
807 Y. Chan and D. R. Blake, *Atmos. Environ.*, 2005, **39**, 5979-5990.
808 91 C. Warneke, J. A. de Gouw, J. S. Holloway, J. Peischl, T. B. Ryerson, E. Atlas, D.
809 Blake, M. Trainer and D. D. Parrish, *J. Geophys. Res.*, 2012, **117**,
810 DOI: 10.1029/2012JD017899.
811 92 J. J. Orlando and G. S. Tyndall, *Chem. Soc. Rev.*, 2012, **41**, 6294-6317.
812 93 M. Sipila, T. Jokinen, T. Berndt, S. Richters, R. Makkonen, N. M. Donahue, R.
813 L. Mauldin, T. Kurten, P. Paasonen, N. Sarnela, M. Ehn, H. Junninen, M. P. Rissanen,
814 J. Thornton, F. Stratmann, H. Herrmann, D. R. Worsnop, M. Kulmala, V. M.
815 Kerminen and T. Petaja, *Atmos. Chem. Phys.*, 2014, **14**, 12143-12153.
816 94 O. Welz, J. D. Savee, D. L. Osborn, S. S. Vasu, C. J. Percival, D. E. Shallcross
817 and C. A. Taatjes, *Science*, 2012, **335**, 204-207.

- 818 95 D. Stone, M. Blitz, L. Daubney, N. U. M. Howes and P. Seakins, *Phys. Chem.*
819 *Chem. Phys.*, 2014, **16**, 1139-1149.
- 820 96 R. A. Cox and S. A. Penkett, *Nature*, 1971, **230**, 321-322.
- 821 97 R. L. Mauldin, T. Berndt, M. Sipila, P. Paasonen, T. Petaja, S. Kim, T. Kurten, F.
822 Stratmann, V. M. Kerminen and M. Kulmala, *Nature*, 2012, **488**, 193-196.
- 823 98 R. Y. Zhang, A. Khalizov, L. Wang, M. Hu and W. Xu, *Chem. Rev.*, 2012, **112**,
824 1957-2011.
- 825 99 M. Kulmala, T. Petaja, M. Ehn, J. Thornton, M. Sipila, D. R. Worsnop and V. M.
826 Kerminen, *Annu. Rev. Phys. Chem.*, 2014, **65**, 21-37.
- 827
- 828